The Cryosphere, 20, 3435–3441, 2026
https://doi.org/10.5194/tc-20-3435-2026
© Author(s) 2026. This work is distributed under
the Creative Commons Attribution 4.0 License.

The Cryosphere
Open Access
EGU

Brief communication: Bed mapping of southern Greenland outlet glaciers using helicopter-borne ground penetrating radar (AIRETH)

Ilaria Santin[1,2], Huw J. Horgan[1,2,3], Raphael Moser[1,2], Nanna Bjørnholt Karlsson[4], Faezeh M. Nick[5], Andreas Vieli[6], Anja Rutishauser[4], Hansruedi Maurer[7], and Daniel Farinotti[1,2]

[1]Laboratory of Hydraulics, Hydrology and Glaciology (VAW), ETH Zürich, Zürich, Switzerland
[2]Swiss Federal Institute for Forest, Snow and Landscape Research (WSL), Sion, Switzerland
[3]Antarctic Research Centre, Victoria University of Wellington, Wellington, New Zealand
[4]Geological Survey of Denmark and Greenland, Copenhagen, Denmark
[5]Faculty of Geosciences, Utrecht University, Utrecht, the Netherlands
[6]Department of Geography, University of Zürich, Zürich, Switzerland
[7]Institute of Geophysics, ETH Zürich, Zürich, Switzerland

Correspondence: Ilaria Santin (santin@vaw.baug.ethz.ch)

Received: 28 January 2026 – Discussion started: 10 February 2026
Revised: 1 May 2026 – Accepted: 14 May 2026 – Published: 16 June 2026

Abstract. Here we present the first southern Greenland deployment of the re-designed Airborne Ice Radar of ETH Zürich (AIRETH). We surveyed a total of 348 km of profiles over three outlet glaciers, identifying basal reflections along 102 km (29 %) of the flight lines. The 25 MHz antennas configuration achieved an effective penetration depth of about 300 m and a maximum measured ice thickness of about 340 m, with bed detectability decreasing over thicker and/or heavily crevassed ice. These results define the depth limitation of our system and show that terrain-following helicopter surveys can provide targeted constraints that complement existing datasets in complex topography.

1 Introduction

The Greenland Ice Sheet is currently losing mass at a rate of $\sim 200\,\mathrm{Gt\,yr^{-1}}$ (IMBIE Team, 2020). This loss reflects the combined effects of surface mass balance and dynamic discharge, with the latter controlled by ice flow speed and ice thickness, particularly across fast-flowing outlet glaciers at the ice-sheet margin (King et al., 2020). While ice velocities can be mapped from remote sensing observations (Moon et al., 2012), ice thickness remains harder to constrain because of the scarcity of measurements.

Ground-penetrating radar (GPR) is effective and established methods for mapping ice thickness (e.g. Schroeder et al., 2020). In Greenland, extensive airborne depth-sounding campaigns were conducted in the frame of NASA's Operation IceBridge (OIB) (Studinger et al., 2010). Using the Multichannel Coherent Radar Depth Sounder (MCoRDS), a high-power, multichannel depth-sounding radar operated from aircraft, OIB achieved deep bed detection at regional scale (Paden et al., 2010). These radar data underpin Greenland ice-thickness and bed-elevation products such as BedMachine (BM), a dataset that combines airborne and ground-based radar thickness measurements (OIB) with surface elevation and ocean bathymetry through a mass-conservation inversion, complemented by interpolation and hydrostatic-equilibrium estimates (Morlighem et al., 2017).

However, southern Greenland still contains gaps in radar-derived thickness coverage, particularly along the coastline and within deep, narrow outlet-glacier corridors (Mouginot et al., 2014). Narrow outlet glaciers can fall between the widely spaced OIB flight lines and, even where crossed, may include segments without reliable bed picks (Fig. 1a, black and grey lines). In addition, rough topography and the liquid water content of temperate ice can increase scattering and signal attenuation, reducing bed detectability, especially for higher-frequency systems (MacGregor et al., 2016).

Here, we report the first deployment of the redesigned, helicopter-borne AIRETH radar system in southern Greenland. We focus on quantifying bed-detection performance in this challenging setting and on assessing how AIRETH bed picks complement the existing OIB and BM ice-thickness products, particularly in complex fjord terrain and near ice-marginal lakes. Our campaign targeted three outlet glaciers on the ice-sheet margin around Narsarsuaq (Fig. 1a), namely: Qooqqup Sermia, Eqalorutsit Kangilliit Sermiat, and Sermilik Bræ. These sites span marine and lake-terminating glaciers in tidewater settings in high-relief terrain, where terrain-following helicopter surveys are advantageous to access the narrow tributaries and ice-marginal lake sectors. In addition, the basal geometry of such sites provides key boundary conditions for both fjord-glacier interactions and lake-related processes (Carrivick et al., 2022). We first summarize the survey and processing workflow, then showing representative GPR profiles and bed-detection success rate, finally comparing AIRETH bed elevations with OIB and BM to illustrate where helicopter-borne GPR adds new constraints.

2 Methods

2.1 AIRETH system

AIRETH (Fig. 1b–c) is a dual-polarization, helicopter-borne GPR system designed for glaciological surveys that has been used extensively in the European Alps (Langhammer et al., 2019; Grab et al., 2021). Our Greenland campaign was conceived as a first deployment under polar conditions and as the first description of the current, redesigned AIRETH configuration. It aimed to assess whether AIRETH can provide measurements in polythermal, fast-flowing and crevassed outlet-glacier terrain.

AIRETH comprises a lightweight modular airframe carrying two commercial PulseEkko radar systems (Sensors & Software). At the core of the system are two orthogonal bistatic dipole antenna pairs operating at central frequencies of 25, 50, or 100 MHz. The radar hardware is controlled by a commercial central unit (SPIDAR pulseEkko Pro NIC-500P) and complemented by an integrated positioning and attitude system composed of (i) four GNSS antennas mounted at the frame corners, (ii) a central inertial measurement unit, and (iii) a laser altimeter providing ground-clearance information (Fig. 1c). System status and acquisition are monitored in real time from the helicopter cockpit.

Compared to earlier AIRETH configurations (Langhammer et al., 2019), the system has been substantially redesigned to improve robustness, positioning and data quality: the original wooden carrier frame was replaced by fibreglass-reinforced plastic beams, reducing total weight by about 60 % (now at 115 kg); the positioning system was integrated to retrieve platform position and orientation during flight; and cable routing was optimized to reduce electromagnetic noise in the GPR signal. Together, these changes yield a self-contained, modular platform and reduced operational constraints. A detailed hardware description of the current AIRETH configuration is provided in Supplement Fig. S1.

2.2 GPR data acquisition and processing

The surveys took place in March 2025, deploying AIRETH in the 25 MHz configuration to maximize the penetration depth. Data were acquired at a target altitude of 30 m above ground, with typical speeds of $\sim 35\,\mathrm{km\,h^{-1}}$ on across-glacier profiles and $\sim 55\,\mathrm{km\,h^{-1}}$ on longitudinal profiles. The few intersections of profiles with clear bed returns were used to assess continuity and internal consistency across individual survey lines. Overall, the collected dataset comprises a total of 348 km of survey lines, encompassing at least one longitudinal profile and several cross profiles for each glacier. The Matlab based GPRglaz package (Grab et al., 2018) was used for data processing. It included two main steps: processing of the positioning data and processing of the GPR data. GNSS, IMU and laser-altimeter data were quality-controlled and combined to obtain platform positions, which were projected onto the glacier surface and synchronized with the GPR traces via GNSS timestamps.

The GPR data were processed following a standard processing workflow to improve signal–to–noise ratio and enable clear interpretation. Processing aims to extract the glacier bed reflections and estimate the ice thickness; it includes: (i) time zero correction based on the arrival of the direct wave, (ii) removal of the ringing noise from helicopter using singular value decomposition filtering, (iii) Butterworth bandpass filtering (10–75 MHz), (iv) trace binning at a constant spatial sampling rate of 1 m for regular sampling, (v) surface reflection picking based on the laser altimetry, (vi) merging the dual-polarization data channels, (vii) time-to-depth conversion by data migration (Kirchhoff and Reverse time migration algorithms), assuming constant radar wave velocities of 0.30 and $0.168\,\mathrm{m\,ns^{-1}}$, for air and ice, respectively. The signal associated with the basal reflection was manually picked in the Petrel software environment (Schlumberger) and the ice thickness was computed as the difference between the elevation of the glacier surface and the elevation of the basal reflections.

2.3 Comparison with existing bedrock estimates

In order to place our results into the context of existing information, we compare them with two available ice thickness and bed elevation constraints: NASA's OIB radar soundings and the BM mass-conservation inversion product (Morlighem et al., 2017). We assess the local consistency between AIRETH and existing constraints using point-wise comparisons at collocated locations.

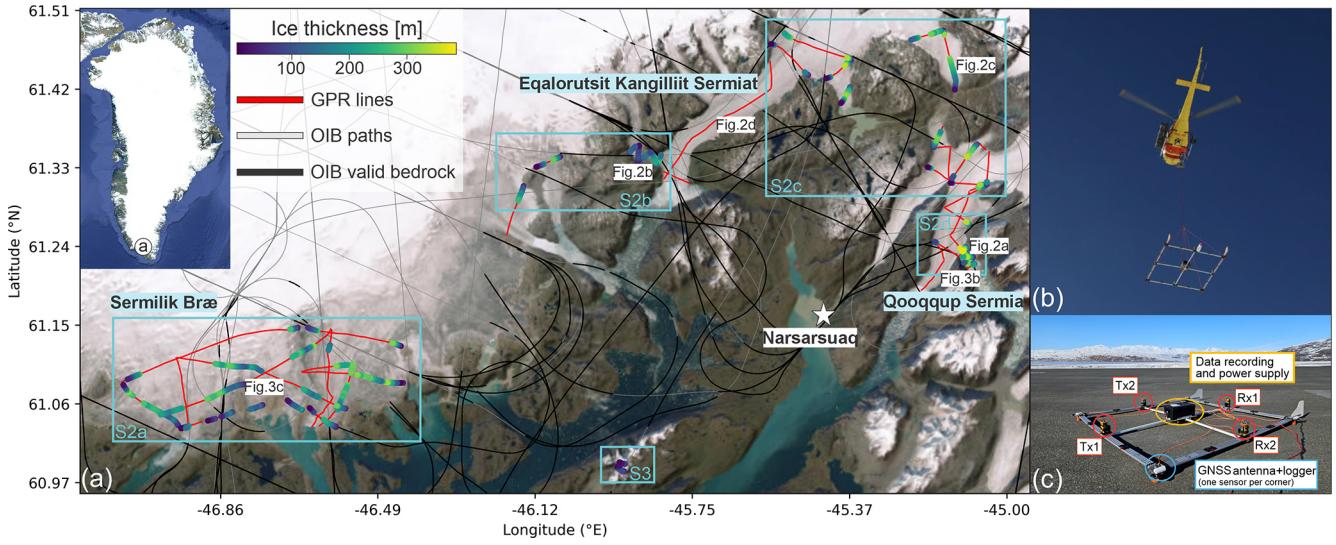

Figure 1. **(a)** Overview of ice thickness data availability in the Narsarsuaq region of Southern Greenland. Red lines: helicopter-borne AIRETH GPR profiles. Grey lines: OIB flight paths; Black segments: OIB samples with valid bed picks. Colored dots along AIRETH lines show ice thickness where the bedrock was interpretetable, while red segment mark zones where it could not be detected. The investigated outlet glaciers Sermilik Bræ, Eqalorutsit Kangilliit Sermiat, and Qooqqup Sermia are labeled. Light-blue squares refer to Supplement Figs. S2 and S3. The white star points to the location of Narsarquaq settlement and airport. Basemap: Esri World Imagery | Powered by Esri. **(b)** AIRETH during acquisition with the carrier frame suspended as a sling-load. **(c)** AIRETH system layout: quad-loop GPR antenna array (two orthogonal Tx–Rx pairs), GNSS antenna + logger, and data-recording/power unit mounted on the carrier frame.

For the comparison with OIB, we used the Level-2 radar product of Paden et al. (2010). We converted the reported one-way surface and bottom ranges to elevations following Paden et al. (2010). Since both datasets are referenced to the WGS-84 ellipsoid, no surface correction is required. For each AIRETH bed pick, we matched OIB soundings (along-track spacing 15 m) within a 10 m horizontal radius and, where multiple valid soundings existed, averaged their bed elevations. Unmatched points were discarded.

For BM comparison, we used BM v5 (NSIDC IDBMG4) from the NSIDC DAAC (Morlighem et al., 2022). We sampled its gridded bed, surface, thickness, and source index at each AIRETH bed-pick location. Within our study region, only 5.5 % of BM grid cells are reported as directly constrained by thickness measurements; the remaining 94.5 % rely on mass-conservation inversion and interpolation.

3 Results and discussion

3.1 AIRETH survey and basal detection in southern Greenland

Bed reflections were identified along about 29 % (102 km out of 348 km) of the AIRETH flight lines, with most bed picks obtained in the Sermilik Bræ and Qooqqup Sermia areas (Fig. 1a). The spatial distribution of bed returns is biased towards shallower glacier margins, whereas bed picks are mainly absent in the thicker central glacier sections. This pattern indicates that basal reflections were most commonly detectable up to ice thicknesses of approximately 300 m, although deeper detections were obtained locally. Only about 5 % of bed picks correspond to ice thicknesses greater than 300 m, and the maximum detected ice thickness is approximately 340 m. At locations without interpretable bed returns, BM indicates thickness higher than 300 m in about 32 % of cases, predominantly along the longer longitudinal profiles. For glacier-scale context and to facilitate identification where bedrock was interpreted, Supplement Figs. S2 and S3 provide zoom-in maps for the glaciers highlighted in Fig. 1a. At some intersections between GPR profiles, a basal reflection is only interpretable along one of the crossing lines. This is not unexpected, because basal detectability depends on profile orientation relative to glacier geometry, as well as on local ice thickness, crevassing, clutter, and out-of-plane reflections from steep valley walls. Kirchhoff migration was applied using the same parameterization for all profiles, independent of survey orientation. However, because migration is applied along individual profiles, it may sharpen the imaging response preferentially in the along-track direction. Differences in flight speed between across-glacier and longitudinal survey modes, which result in different along-track trace densities prior to stacking, may further affect local signal quality and thus basal-reflection interpretability. As a result, the glacier bed may be interpretable along one profile but not along another, even at nearby crossings. Such differences do not necessarily imply inconsistent interpretation but rather reflect variable imaging conditions and data quality.

Longitudinal lines are frequently uninterpretable over deeply crevassed and thicker ice, where the 25 MHz antenna lacked penetration and thus coherent basal returns (Fig. 2d). By contrast, cross-glacier profiles are more reliable, benefitting from tie points at rock outcrops along the margins.

The basal interface presents substantial variability in radar expression across the surveyed glaciers. In several profiles, it appears as a transition from low-amplitude, texture-like clutter to a zone of persistently higher backscatter (Fig. 2a), whereas in others it forms a clearer and more laterally continuous high-amplitude horizon (Fig. 2c). Some profiles also show strong scattering immediately above the basal reflection, which is nevertheless still clearly recognizable (Fig. 2b). Bed picking was adapted to the local radar expression and guided by lateral continuity, targeting the deepest laterally coherent basal signal or the onset of persistent enhanced backscatter at the base of the ice thickness. Where no such criterion could be met, no bed pick was assigned. Internal englacial reflectors are generally absent in the 25 MHz data. An exception is the relatively thin Narsaq Bræ (Supplement Fig. S3; location in Fig. 1a), where profiles show a distinct internal scattering zone at about 20 m depth that is consistent with a cold–temperate ice transition within the glacier (Supplement Fig. S3b).

3.2 Comparison to OIB and BM estimates

To assess consistency with existing estimates and place AIRETH picks (referred to as "GPR" here below) into context, we compare bed elevations at crossings with OIB and at collocated points with BM. At the intersections of OIB and GPR, bed elevations mostly follow the 1 : 1 line (red dots in Fig. 3a). The median bed difference is about +7 m, which is comparable to our point-wise GPR bed-elevation uncertainty (13 and 22 m for depths of 100 and 400 m, respectively; see Appendix A2). A subset of points departs from this pattern, with OIB indicating bed elevations up to about 390 m lower than AIRETH at a few crossings in the Qooqqup Sermia sector. On the contrary, OIB generally yields higher bed elevations than GPR around Sermilik Bræ.

Comparison between GPR and BM bed points show a broad scatter around the 1:1 line (Fig. 3a; blue dots). Many points lie below the 1 : 1 line, meaning that AIRETH tends to indicate a lower bed than BM. Moreover, a non-negligible number of AIRETH points are higher than the BM estimate, though. The spread increases with depth and includes spatially coherent clusters deviating in both directions. Overall, the bed difference $\Delta\text{bed} = \text{bed}_{\text{GPR}} - \text{bed}_{\text{BM}}$ has a median of −126 m (mean −92 m). A representative profile (Fig. 3b) illustrates a case where BM is more than 300 m deeper than our interpretation at the deepest point, despite a broadly similar bed shape.

The surface offset $\Delta s = \text{surf}_{\text{GPR}} - \text{surf}_{\text{BM}}$ has a median of −4.9 m, a mean of −2.5 m, and a standard deviation of 21 m, i.e. a few tens of metres at most. These offsets are thus much smaller than the bed differences reported in Appendix A2, meaning that surface-elevation differences are not the dominant source of the AIRETH–BM mismatch. Rather than attempting a detailed attribution of these discrepancies, we simply note that bedrock elevations from different products can differ by up to a few hundred metres locally, even where surface elevations agree within a few meters.

3.3 AIRETH as a complement to existing datasets

The above comparisons highlight that helicopter-borne GPR can complement existing products by spatial filling gaps, and by targeting complex marginal terrain and narrow outlet-glacier corridors, at least within the penetration range of the current 25 MHz setup. In our study area, AIRETH and existing products show broadly consistent bed elevations at many locations, although local large mismatches of up to a few hundred meters occur. At the same time, the BM source index indicates that only a small fraction of the BM grid cells are directly constrained by thickness measurements, meaning that local differences should be interpreted with care. In the Sermilik Bræ sector, BM is directly constrained by radar-derived ice-thickness measurements only along a few flight segments (black lines in Fig. 1a); elsewhere it relies on the inversion between tracks without such data. Similarly, in the northern part of the survey, near Eqalorutsit Kangilliit Sermiat, AIRETH provides additional bed measurements along outlet-glacier trunks where OIB lines are sparse. More generally, we argue that helicopter-borne GPR can supply targeted thickness measurements where outlet glaciers are otherwise unconstrained, particularly in shallower ice conditions. Similarly, such surveys could be applied elsewhere to densify bed observations in regions with sparse or no radar coverage.

Our surveys help to quantify bed-detection performance and practical limitations of the current AIRETH setup. Using a 25 MHz center frequency, bed reflections are generally retrieved up to depths in the order of 300 m (only ∼ 5 % of picks are deeper), whereas attenuation and scattering increasingly mask the bed signal in thicker, crevassed ice, particularly along longitudinal profiles. A lower-frequency configuration (e.g. 12.5 MHz) could extend this depth range, at the expense of vertical resolution. Although higher transmit power could also improve penetration, it is not freely adjustable due to hardware constraints and radio-frequency/aviation regulations. On the positive side, the helicopter platform permits slow flight speeds and tight manoeuvring, enabling dense stacking and targeted coverage in complex glacier geometry. AIRETH can thus be valuable in filling gaps in existing ice thickness products despite its current depth limitation.

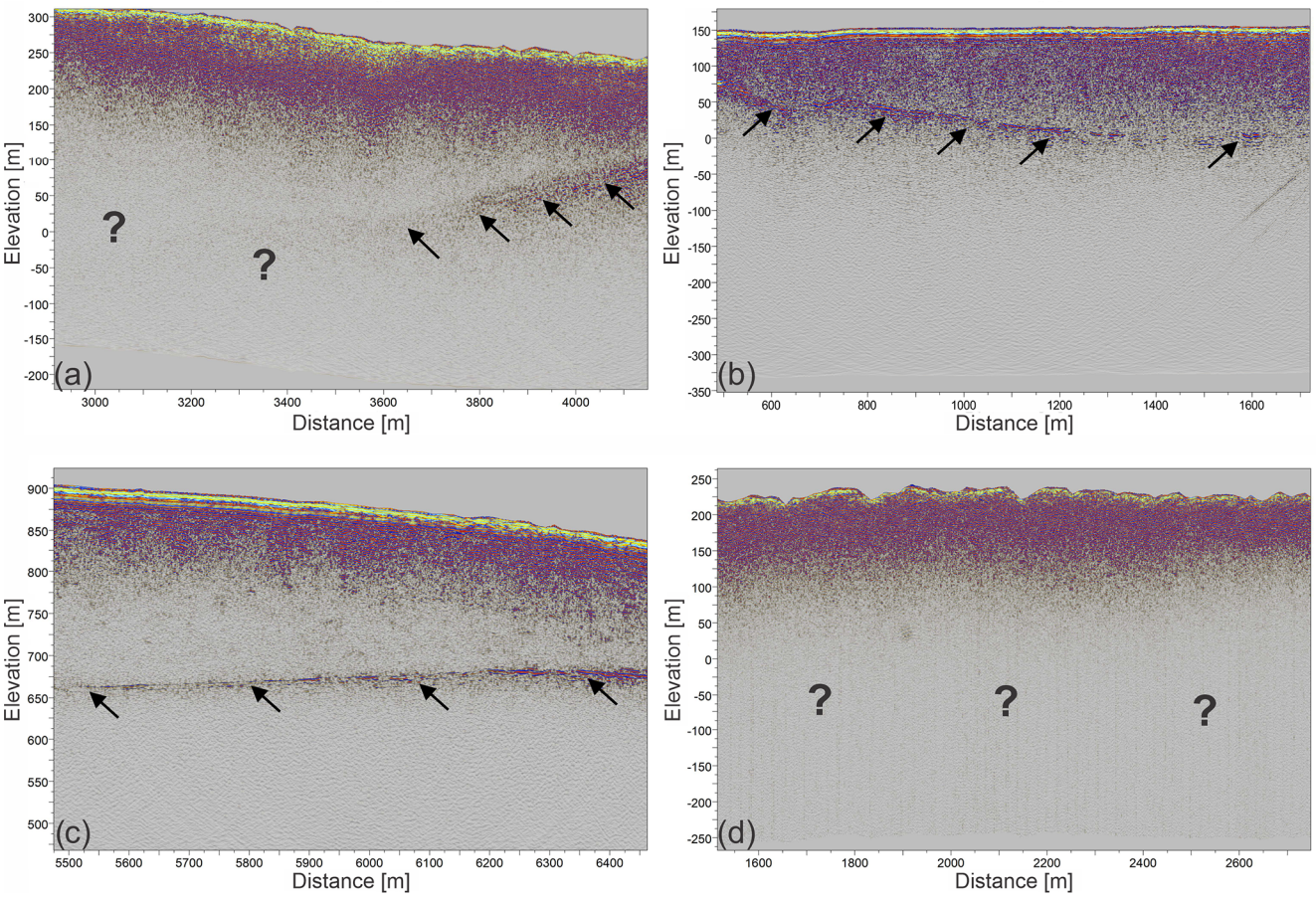

Figure 2. (a–d) Examples of 25 MHz radar sections. Black arrows mark the interpreted bed, while question marks highlight sectors with no reliable basal return. For profiles location, see Fig. 1a.

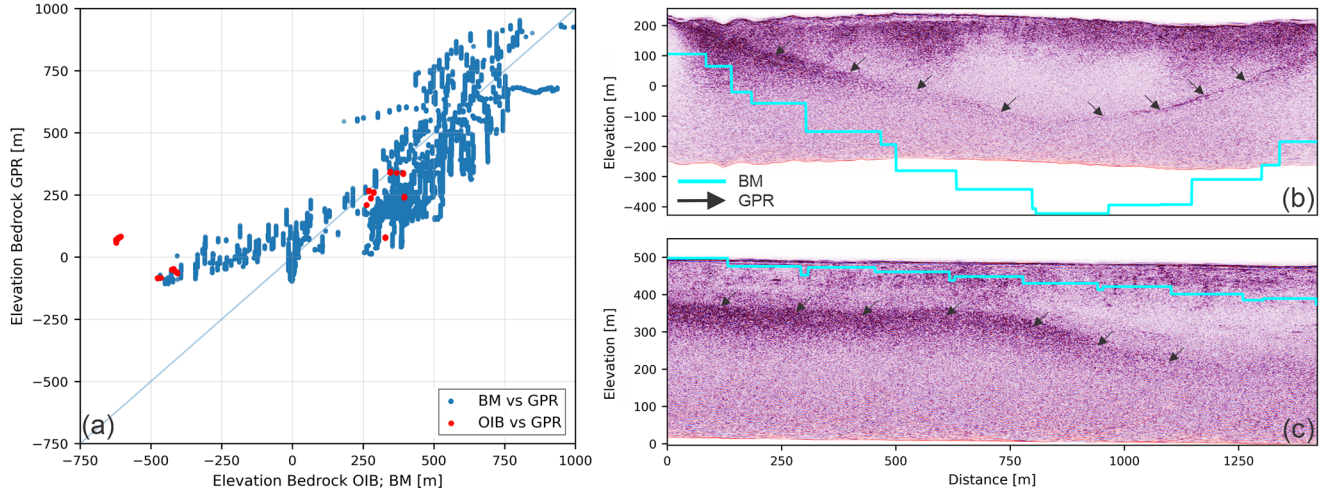

Figure 3. (a) Scatterplot of AIRETH-derived bedrock elevations compared to BM (blue) and OIB (red). The pale diagonal represents the 1 : 1 line. **(b, c)** Representative GPR profiles showing the mismatch between the bed identified in AIRETH profiles (black arrows) and BM (light blue line). For profile location, see Fig. 3a.

4 Conclusions

Our AIRETH survey in southern Greenland shows that a 25 MHz helicopter-borne GPR can recover the ice thickness along about 29 % of the flown profiles (102 km out of 348 km), retrieving thickness values up to about 340 m. Relative to existing datasets, these new bed picks provide direct thickness constraints in under-sampled outlet-glacier corridors and can therefore support refinement of gridded ice-thickness products in such areas. The survey also constrains the practical operating range of the current AIRETH configuration. At 25 MHz, bed reflections are typically retrieved up to depths of ~ 300 m, with only about 5 % of picks in thicker ice. This provides a first estimate of the usable depth window. Future deployments will explore a lower-frequency setup (12.5 MHz) to extend penetration depth, acknowledging the associated trade-off in vertical resolution while retaining the flexibility of the helicopter-borne platform. After conducting tests on larger and heavier lower-frequency antennas, targeted surveys of this type could support selective mapping of ice thickness in other polar regions, and contribute to the goals of the UN Decade of Action for the Cryosphere Sciences (2025–2034).

Appendix A: Estimation of GPR uncertainties

Since interpretable basal reflections were sparse in our dataset, no interpolation was performed between profiles. Uncertainties therefore refer to pointwise bed elevations and include contributions from vertical referencing, the assumed radar-wave velocity in ice, and bed interpretability.

For the vertical referencing, we determine a crossing-point surface mismatch of $\mathrm{err}_z \approx 6$ m, estimated as the standard deviation of surface-elevation differences at line intersections. This metric captures uncertainties in georeferencing, surface roughness, small horizontal mismatches over sloping terrain, and slight differences in frame tilt between different flight directions.

In the absence of site-specific constraints for the radar-wave velocity in ice, we use $v = 0.168 \pm 0.008\,\mathrm{m\,ns^{-1}}$ (Grab et al., 2021). If ice is significantly wetter than assumed, effective velocities may be lower than $0.168\,\mathrm{m\,ns^{-1}}$, which would systematically reduce thickness, and thus bed depth, estimates in direct proportion to v. For instance, using $v = 0.160\,\mathrm{m\,ns^{-1}}$ would decrease thickness by $\sim 5\,\%$. The velocity-related uncertainty $\mathrm{err_v}(h)$ scales linearly with depth h as

$$\mathrm{err_v}(h) = \frac{0.008}{0.168}\,h \approx 0.047\,h. \tag{A1}$$

To account for diffuse or ambiguous basal returns, we adopt a conservative picking uncertainty of $\mathrm{err_p} = 10$ m, informed by the "ambiguous bed" class in Grab et al. (2021) and rounded to reflect our common bed appearance. Assuming independent uncertainties and combining these terms in quadrature, the pointwise bed-elevation uncertainty $\mathrm{err_{bed}}(h)$ is

$$\mathrm{err_{bed}}(h) = \sqrt{\mathrm{err}_z^2 + \mathrm{err_v}(h)^2 + \mathrm{err_p}^2}. \tag{A2}$$

Based on Eq. (A2), $\mathrm{err_{bed}}(h)$ is ~ 13, 15, 18 and 22 m for depths of $h = 100$, 200, 300 and 400 m, respectively. Equation (A2) should be interpreted as a lower bound for intervals with ambiguous basal returns, where diffuse or multi-peaked reflections can increase the picked horizon beyond $\mathrm{err_p}$.

Data availability. Basal reflection picks are available at https://doi.org/10.3929/ethz-c-000794464 (Santin et al., 2025a). The corresponding AIRETH radar data are available at https://doi.org/10.3929/ethz-c-000799347 (Santin et al., 2025b).

Supplement. The supplement related to this article is available online at https://doi.org/10.5194/tc-20-3435-2026-supplement.

Author contributions. Conceptualization: DF, NBK, FMN, AV, AR, HM. Survey planning: IS, RM, DF. Data acquisition: RM, DF. Data processing: IS, RM. Data interpretation: IS with contributions from HH, HM. Manuscript writing: IS with contributions from all co-authors.

Competing interests. At least one of the (co-)authors is a member of the editorial board of *The Cryosphere*. The peer-review process was guided by an independent editor, and the authors also have no other competing interests to declare.

Disclaimer. Publisher's note: Copernicus Publications remains neutral with regard to jurisdictional claims made in the text, published maps, institutional affiliations, or any other geographical representation in this paper. The authors bear the ultimate responsibility for providing appropriate place names. Views expressed in the text are those of the authors and do not necessarily reflect the views of the publisher.

Acknowledgements. We acknowledge Schlumberger for the ETH Zürich Petrel® academic license. We acknowledge Thomas Teisberg and Emanuele Forte for their constructive reviews.

Financial support. This research has been supported by the Carlsbergfondet (grant no. CF24-2350).

Review statement. This paper was edited by Stephen Livingstone and reviewed by Emanuele Forte and Thomas Teisberg.

References

Carrivick, J. L., How, P., Lea, J. M., Sutherland, J. L., Grimes, M., Tweed, F. S., Cornford, S., Quincey, D. J., and Mallalieu, J.: Ice-Marginal Proglacial Lakes Across Greenland: Present Status and a Possible Future, Geophys. Res. Lett., 49, e2022GL099276, https://doi.org/10.1029/2022GL099276, 2022.

Grab, M., Bauder, A., Ammann, F., Langhammer, L., Hellmann, S., Church, G., Schmid, L., Rabenstein, L., and Maurer, H.: Ice volume estimates of Swiss glaciers using helicopter-borne GPR – an example from the Glacier de la Plaine Morte, in: 2018 17th International Conference on Ground Penetrating Radar (GPR), 1–4, https://doi.org/10.1109/ICGPR.2018.8441613, 2018.

Grab, M., Mattea, E., Bauder, A., Huss, M., Rabenstein, L., Hodel, E., Linsbauer, A., Langhammer, L., Schmid, L., Church, G., Hellmann, S., Délèze, K., Schaer, P., Lathion, P., Farinotti, D., and Maurer, H.: Ice thickness distribution of all Swiss glaciers based on extended ground-penetrating radar data and glaciological modelling, J. Glaciol., 67, 1074–1092, https://doi.org/10.1017/jog.2021.55, 2021.

IMBIE Team: Mass balance of the Greenland Ice Sheet from 1992 to 2018, Nature, 579, 233–239, https://doi.org/10.1038/s41586-019-1855-2, 2020.

King, M. D., Howat, I. M., Candela, S. G., Noh, M. J., Jeong, S., Noël, B. P. Y., van den Broeke, M. R., Wouters, B., and Negrete, A.: Dynamic ice loss from the Greenland Ice Sheet driven by sustained glacier retreat, Commun. Earth Environ., 1, 1–7, https://doi.org/10.1038/s43247-020-0001-2, 2020.

Langhammer, L., Grab, M., Bauder, A., and Maurer, H.: Glacier thickness estimations of alpine glaciers using data and modelling constraints, The Cryosphere, 13, 2189–2202, https://doi.org/10.5194/tc-13-2189-2019, 2019.

MacGregor, J. A., Fahnestock, M. A., Catania, G. A., Aschwanden, A., Clow, G. D., Colgan, W. T., Gogineni, P. P., Morlighem, M., Nowicki, S. M. J., Paden, J. D., Price, S. F., and Seroussi, H.: A synthesis of the basal thermal state of the Greenland Ice Sheet, J. Geophys. Res.-Earth, 121, 1328–1350, https://doi.org/10.1002/2015JF003803, 2016.

Moon, T., Joughin, I., Smith, B., and Howat, I.: 21st-century evolution of Greenland outlet glacier velocities, Science, 336, 576–578, https://doi.org/10.1126/science.1219985, 2012.

Morlighem, M., Williams, C. N., Rignot, E. J. M., An, L., Arndt, J. E., Bamber, J. L., Catania, G. A., Chauché, N., Dowdeswell, J. A., Dorschel, B., Fenty, I., Hogan, K. A., Howat, I. M., Hubbard, A., Jakobsson, M., Jordan, T. M., Kjeldsen, K. K., Millan, R., Mayer, L., Mouginot, J., Noël, B. P. Y., O'Cofaigh, C., Palmer, S. J., Rysgaard, S., Seroussi, H., Siegert, M. J., Slabon, P., Straneo, F., van den Broeke, M. R., Weinrebe, W., Wood, M., and Zinglersen, K. B.: BedMachine v3: Complete bed topography and ocean bathymetry mapping of Greenland from multi-beam echo sounding combined with mass conservation, Geophys. Res. Lett., 44, https://doi.org/10.1002/2017GL074954, 2017.

Morlighem, M., Williams, C. N., Rignot, E. J. M., An, L., Arndt, J. E., Bamber, J. L., Catania, G. A., Chauché, N., Dowdeswell, J. A., Dorschel, B., Fenty, I., Hogan, K. A., Howat, I. M., Hubbard, A., Jakobsson, M., Jordan, T. M., Kjeldsen, K. K., Millan, R., Mayer, L., Mouginot, J., Noël, B. P. Y., O'Cofaigh, C., Palmer, S. J., Rysgaard, S., Seroussi, H., Siegert, M. J., Slabon, P., Straneo, F., van den Broeke, M. R., Weinrebe, W., Wood, M., and Zinglersen, K. B.: IceBridge BedMachine Greenland (IDBMG4, Version 5), Dataset, https://doi.org/10.5067/GMEVBWFLWA7X, 2022.

Mouginot, J., Rignot, E., Gim, Y., Kirchner, D., and Le Meur, E.: Low-frequency radar sounding of ice in East Antarctica and southern Greenland, Ann. Glaciol., 55, 138–146, https://doi.org/10.3189/2014AoG67A089, 2014.

Paden, J., Li, J., Leuschen, C., Rodríguez-Morales, F., and Hale, R.: IceBridge MCoRDS L2 Ice Thickness, Version 1, Dataset, updated 2019, https://doi.org/10.5067/GDQ0CUCVTE2Q, 2010.

Santin, I., Farinotti, D., and Moser, R.: Ice thickness measurements from Southern Greenland (2025) using helicopter-borne ice-penetrating radar (AIRETH), ETH Zurich [data set], https://doi.org/10.3929/ethz-c-000794464, 2025a.

Santin, I., Farinotti, D., and Moser, R.: Ground-penetrating radar data from Southern Greenland (2025) acquired using the helicopter-borne AIRETH system, ETH Zurich [data set], https://doi.org/10.3929/ethz-c-000799347, 2025b.

Schroeder, D. M., Bingham, R. G., Blankenship, D. D., Christianson, K., Eisen, O., Flowers, G. E., Karlsson, N. B., Koutnik, M. R., Paden, J. D., and Siegert, M. J.: Five decades of radioglaciology, Ann. Glaciol., 61, 1–13, https://doi.org/10.1017/aog.2020.11, 2020.

Studinger, M., Koenig, L., Martin, S., and Sonntag, J.: Operation IceBridge: Using instrumented aircraft to bridge the observational gap between ICESat and ICESat-2, in: 2010 IEEE International Geoscience and Remote Sensing Symposium (IGARSS), 1918–1919, https://doi.org/10.1109/IGARSS.2010.5650555, 2010.